Optical Parameters of Varies Thickness of Bismuth (Iii) Iodide Thin Films for Photovoltaic and Nonlinear Applications

M. Salah, A. M. Abdelnaeim, S. A. Makhlolf, A. EL-Taher and E. R. Shaaban*

Physics Department, Faculty of Science, Al-Azhar University, Assiut 71524, Egypt

Abstract: We report in varies thickness of BiI_3 thin films by thermal evaporation techniques onto glass substrate. The films were strongly oriented along the (113) plane. The structural parameters of these films (crystallite size and lattice strain) were determined using (XRD) pattern. The thicknesses and refractive indices of the films were considered using Swanepoel's method. The band gap was determined in terms of T and R spectrum in the UV-region of the absorption. The possible optical transitions of all films are found to be allowed direct transition with energy gap fluctuate bout $1.96 \pm 2\%$ eV. Dielectric constant, volume-energy-loss function (VELF) and surface-energy-loss function (SELF) for as deposited films were discussed in terms of film thickness rising. The change in optical parameters have been interpreted in terms of the change in microstructure parameters. BiI3 is recommended for photovoltaics and nonlinear optics because of its higher absorption coefficient, dielectric constant, and fair band gap.

1 Introduction

BiI_3 has the space group R-3h and is a layered compound. That is, it possesses a rhombohedral/trigonal lattice with iodine atoms in the lattice points and bismuth cations filling two-thirds of the octahedral holes [1]. Because the trigonal crystal system is a member of the hexagonal crystal family, joining BiI_3 unit cells results in a hexagonal crystal system. A hexagonal structure is formed in three dimensions. layered semiconductor nanoparticles as BiI_3, PbI_2, HgI, and MoS_2 are with potential uses in photovoltaics, detectors, sensors, photocatalysis, lubrication, nonlinear optics, and photo-electrochemistry. They have benefits such as improved transport characteristics (inside a layer), fewer defects due to virtually perfect surfaces with almost no dangling bond perpendicular to the layer, and significant visual absorption due to tiny band gaps [2-4]. Many works have been done on BiI_3 based on its structural [5], electronic [6, 7] and optical [8-11] features. Krylova et al. [12] studied the absorption and luminescence spectra of BiI_3 crystals in a low temperature range (1.6–77 K). H. Kondo et al [13] also investigated the luminescence characteristic of BiI_3. Thin films of BiI_3 have been studied for hard radiation detection and for X-ray imaging because of the quite wide band gap (1.67 eV) [14] and great mass density [15-17]. Also, BiI_3 has been utilized as a nanoscale

pressure sensor [18] and a photo-detector [19]. The current work reports the investigation of structural and optical features of Bismuth iodide (BiI_3) nanocrystalline thin films with different thicknesses. Since the thermal evaporation technique is used to obtain different thicknesses of BiI_3 thin films. XRD is used to investigate the structural parameters of the studied thin films. The optical characterization is obtained using double beam Uv/Vis Spectrophotometer. The films thicknesses and subsequently the other optical constants are measured accurately according to Swanepoel method.

The current work focuses on: (1) using the Scherrer and Wilson equations to calculate structural parameters (crystallise size and lattice strain) of different thicknesses of BiI_3, (2) using the developed envelope equations for maximum and minimum to calculate thickness and refractive index, as suggested by Swanepoel, (3) calculating the dielectric constants, volume energy, surface energy, energy gap and nonlinear refractive index for photovoltaic and nonlinear optics and (4) interpreting changes in optical parameters in terms of structural parameters.

2 Experimental procedures

BiI_3 was acquired from Sigma Aldrich and utilized as supplied, with no additional purification. BiI_3 thin films of

*Corresponding author E-mail: esam_ramadan2008@yahoo.com

varying thicknesses were evaporated on clean glass substrates using a thermal evaporation equipment (type E-306A, England). The base vacuum pressure was around 10^{-6} Pa. A quartz crystal monitor (FTM4, Edwards) is supplied with the coating equipment to determine the rate of deposition and adjust the film thickness throughout the evaporation process. At room temperature, the substrate temperature remained constant. To avoid any heating impact through the preparation of BiI_3 layer, the distance between the boat of the sample and the holder of substrate was set at 21 cm. The (XRD) pattern of the films was determined using a Philips diffractometer (model-X-pert) by using target CuK_a radiation at wavelength $\lambda = 1.5418$ Å. Both optical transmittance (T) and reflectance (R) of BiI_3 thin films were measured by using a dual spectrophotometer (JASCO, V-670 UV–VIS–NIR).

3 Results and discussion
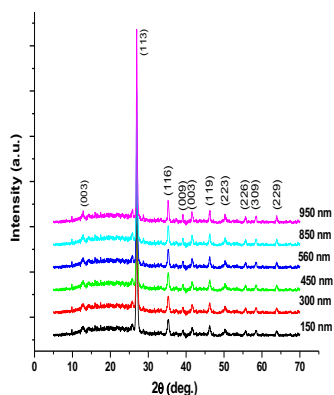
3.1 XRD analysis

Fig. 1: The XRD patterns of BiI_3 with different thicknesses.

Fig. 1 demonstrates XRD patterns of different thicknesses of BiI_3 thin films. Such figure revealed sharp peaks which identify the crystalline nature of all the investigated films. According to Rietveld refinement method, the investigated crystalline material was characterized [20]. Fig. 1 displays the diffraction peaks for the as-deposited BiI_3 films of different thicknesses in the XRD pattern that belong to (JCPDS Data File: 00-048-1795 Rhombohedral) structure with preferred orientation along the (113) plane. For diffraction angle values $2\theta = 12.825$, 27, 39.125, 41.645, 46.285, 50.325, 55.765, 58.325 and 63.905 corresponding to (003), (113), (116), (009), (003), (119), (223), (226), (309) and (229) oriented planes respectively, this corresponded well with literature [11, 21]. Fig. 1 also shows that as the films thickness of BiI_3 thin films increases

the diffracted strength of (113) plane increases, which reveal to the improvement of the crystallization competence of deposited films with rising their thickness.

The microstructure parameters, crystallize size, D_v, and lattice strain, ε, are calculated by the Scherrer and Wilson equations [22-24]:

$$D = \frac{0.9\lambda}{\beta \cos\theta} \qquad (1)$$

$$e = \frac{\beta}{4\tan\theta} \qquad (2)$$

where $\lambda = 1.54$ Å is the wavelength, and the broadening width of the peak β is estimated through the relation:

$$\beta = \sqrt{\beta_{obs}^2 - \beta_{std}^2}$$

where β_{obs} and and β_{std} are the corresponding peak widths of the film and standard (silicon), respectively.
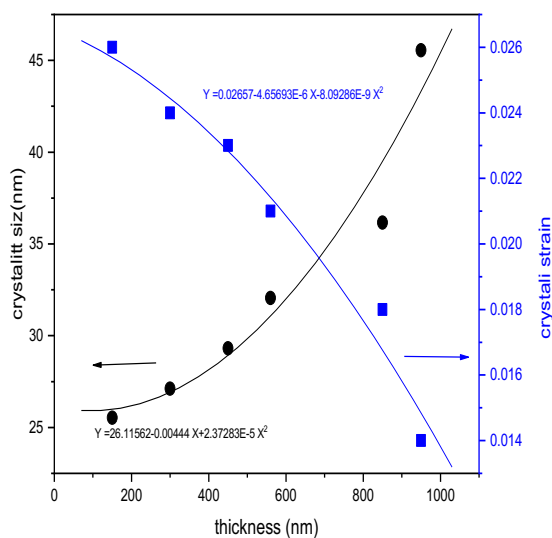

Fig. 2: Variations of the microstructural parameters on BiI_3 thin films

Fig. 2 shows (D and e) of the BiI_3 films of various thicknesses. It is detected that the average crystallite size increases (27 nm – 47 nm nearly) with growing the film thickness, but the lattice strain shrinkages. Fig. 2 presents a comparison of the (D and e) of the BiI_3 films of different thicknesses varies between 150 nm and 950 nm. The observed behavior of microstrain may be owing to growth

in crystallite size. Such a reduction in the lattice strain reveals the diminution in the lattice imperfections.

3.2. Optical analysis

3.2.1 Refractive index and energy gap

Double beam spectrophotometer can be used to get the spectral dependence of the optical (T) and (R) of the as deposited films.
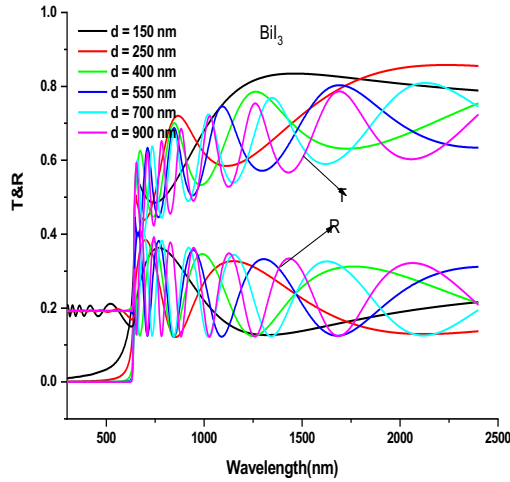

Fig. 3: Transmission and reflection spectra of BiI₃ with different thicknesses thin films.

Fig. 3 illustrates the variation of the absolute of $T(\lambda)$ and $R(\lambda)$ values versus λ. The occurrence of interference and the presence of maxima and minima in the transmission spectrum confirmed these BiI₃ thin films have excellent quality and homogeneity. The n value was calculated using Swanepoel's method. This method has envelopes of recording around the maximum and minimum of the transmission spectrum [25-27].

New functions have been used to express mathematically the maximum transmission $T_M(\lambda)$ and the minimum transmission $T_m(\lambda)$ as the next

$$T_M(\lambda) = T_{01} + A_{11}.\exp\left[-\frac{\lambda}{t_{11}}\right] + A_{12}.\exp\left[-\frac{\lambda}{t_{12}}\right] \quad (3)$$

$$T_m(\lambda) = T_{02} + A_{21}.\exp\left[-\frac{\lambda}{t_{21}}\right] + A_{22}.\exp\left[-\frac{\lambda}{t_{22}}\right] \quad (4)$$

The constants values of the two equations namely, T_{01}, A_{11} t_{11}, A_{12} and t_{12} (Eq. 3) or T_{02}, t_{21}, A_{21}, A_{22} and t_{22} (Eq. 4) are summarized Table 1.

According to this method the n value can be considered at a given λ using the next equation [25, 26, 28].

$$n_j(\lambda) = 2s.\left[\frac{(T_M - T_m)}{(T_M T_m)}\right] + \left[\frac{s^2+1}{2}\right] + \sqrt{\{2s.\left[\frac{(T_M - T_m)}{(T_M T_m)}\right] + \left[\frac{s^2+1}{2}\right]\}^2 - s^2} \quad (5)$$

T_M and T_m at a certain wavelength are the maximum transmittance and the corresponding minimum. Additionally, both envelopes were calculated using the Origin program (Corp. Origin Lab) (see Fig. 4).
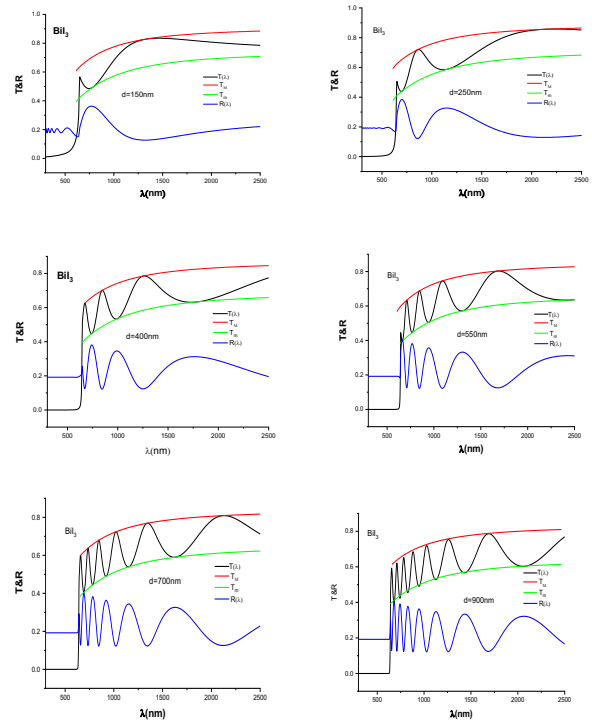

Fig. 4: Variation of the typical spectral transmittances vs. wavelength for BiI₃ thin films indicating to the created envelopes as mentioned in text.

Furthermore, the required values for the refractive index of the substrate can be computed using transmission of the substrate, T_S using the equation [29]:

$$s = \frac{1}{T_s} + \left(\frac{1}{T_s} - 1\right)^{\frac{1}{2}} \quad (6)$$

Where $T_s(\lambda) = [A + B\lambda + C\lambda^2 + D\lambda^3]$ and constants A, B, C and D equal to 0.901414, 8.02369x10⁻⁵, 6.13838x10⁻⁸ and 1.38877x10⁻¹¹, respectively.

The initial values of refractive index are deduced and fitted according to Cauchy relationship, $n(\lambda) = a + (b/\lambda^2)$ which can be used to extrapolate the entire wavelengths. The variations of refractive index n dispersion relation of BiI₃ thin films of different thicknesses are shown in Fig. 5.
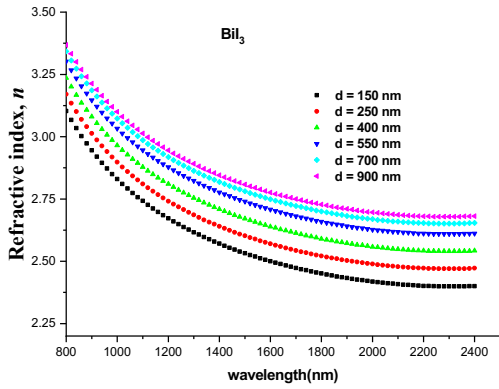
Fig. 5: The spectral dependence of refractive index, *n* for BiI₃ thin films.

It is clearly shown in Fig. 5 that the *n* decreases with increasing wavelength for all the investigated thin films but also the refractive index increases with increasing the film thickness at all values of λ which can be interpreted in increasing the crystallite size of these films. Furthermore, if n_1 and n_2 are the refractive indices at two adjacent maxima (or minimum) at λ_1 and λ_2, the equation of determine the film thickness is:

$$d_1 = \frac{A}{2}.(\lambda_1.\lambda_2) \times [\lambda_1 n_2 - \lambda_2 n_1]^{-1} \qquad (7)$$

The determined thicknesses of the BiI₃ thin films were 150, 250, 400, 550, 700, 900 nm, respectively.

The absorption coefficient, α can be determined form R and *T* values from the following expression [29, 30]:

$$\alpha = \frac{1}{d} \ln\left[\frac{(1-R)^2 + \left[(1-R)^4 + 4R^2T^2\right]^{1/2}}{2T} \right] \qquad (8)$$

where *d* is the film thickness. Fig. 6 shows the reliance of α(*hν*) on photon energy for varies film thickness. It is clear in Fig. 6 that the fundamental absorption edge which related to the optical band gap have higher values greater than 10^5 cm^{-1} for all the investigated films which confirm the ability of using these films in various optoelectronic applications.
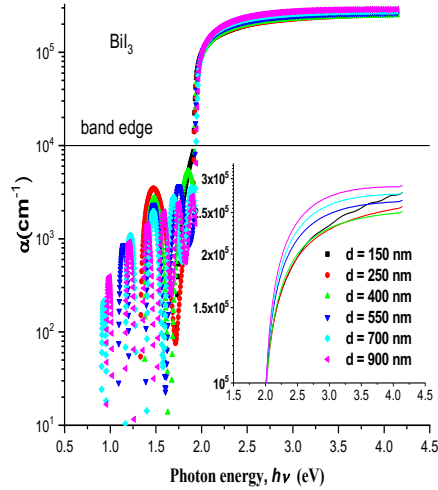

Fig. 6: The dependence of the absorption coefficient on the incident photon energy for BiI₃ thin films.

It is known that the α(*hν*) is described in the neighborhood of the central absorption edge, for allowing direct transitions as follows [31].

$$\alpha(h\upsilon) = \frac{K(h\upsilon - E_g^{opt})^m}{h\upsilon} \qquad (9)$$

Where K is a characteristic parameter for the transitions [30], E_g^{opt} is the energy gap, and m is a number that characterizes the transition. m = 1/2 for crystalline semiconductors (direct transition). Fig. 7 is the best fit of (αhν)² vs. (hν) for BiI₃ films with different thicknesses.

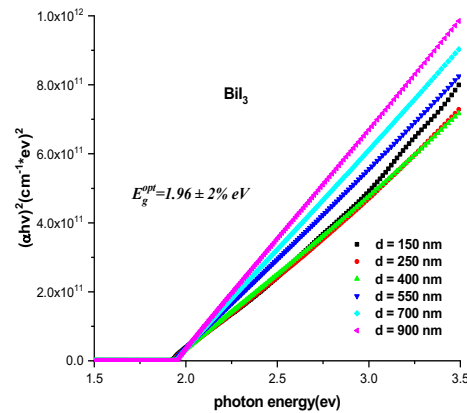**Fig. 7: The plot of (α.hν)² versus photon energy, (hν) for BiI₃ thin films.**

The direct optical band gap E_g^{opt} was taken as the

intercept of $(\alpha . h\nu)^2$ vs. $(h\nu)$ at $(\alpha h\nu)^2 = 0$ for the allowed direct transition. The determined optical energy gap was about $1.96 \pm 2\%$ eV. Now, we will deal with the so-called second absorption constant, namely the extinction coefficient, (k). that can be computed using the next equation [30]:

$$k = \alpha\lambda/4\pi \quad (10)$$

Fig. 8. shows that the values of extinction coefficient, (k_{ex}) of investigated films firstly increase with increasing wavelength until reaching to 500 nm then they decrease with increasing wavelength up to 2500 nm which related to the increasing probability of absorption processes in the lower wavelength range.
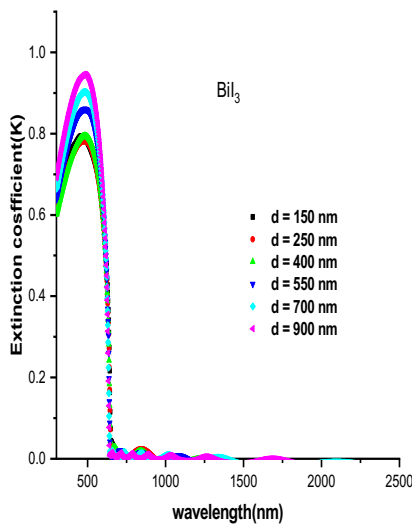

Fig. 8: Variation of extinction coefficient, *(k)* vs. wavelength, *(λ)* for BiI₃ thin films.

3.2.2 Dielectric constants

Dielectric constant is the influences the electromagnetic radiation that passes through the film. As given below as the complex dielectric function [30]

$$\varepsilon = \varepsilon_1 + i\,\varepsilon_2 \quad (11)$$

where ε_1 is the part of the dielectric constant associated with the process of slowing down the light speed in the material. ε_2 is the imaginary part of the dielectric constant which covers the way for the absorption of energy from the electric field by dipole movement. This also applies to the n and k as,

$$\varepsilon_1 = n^2 - k^2 \quad (12)$$

$$\varepsilon_2 = 2nk \quad (13)$$

The variations of ε_1 and ε_2 versus wavelength function are shown in Fig. 9 and Fig. 10 respectively. The dielectric constants are shown to be lessening with increasing the wavelength whereas increasing with cumulative the film thickness which may be attributed to increasing the crystallite size.
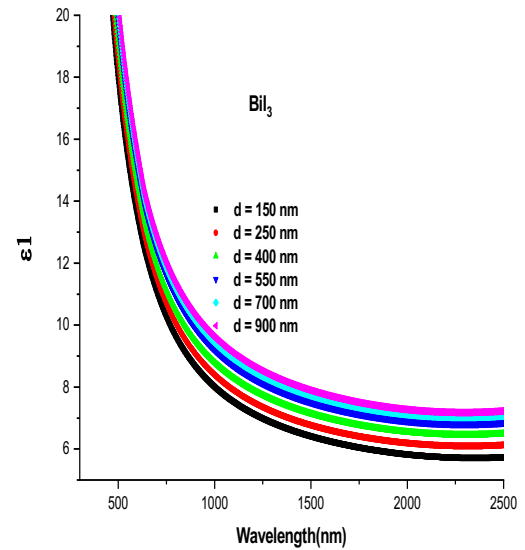

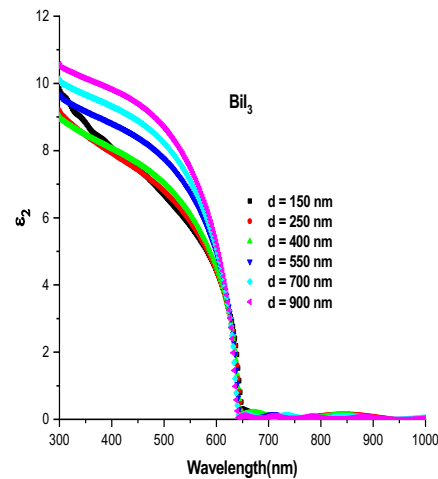**Fig. 9: Variation of real dielectric constant, ε_r on wavelength, λ for BiI₃ thin films.**

Fig. 10: Variation of imaginary dielectric constant, ε_i on wavelength, λ for BiI₃ thin films.

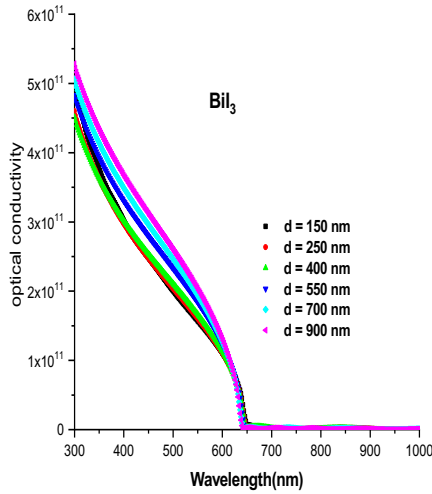### 3.2.3 Determination of the optical conductivity

Fig. 11: Dependence of optical conductivity, σ_{opt} as a function of wavelength λ for BiI₃ thin films.

Fig. 11 shows the discrepancy of optical conductivity, $\sigma_{opt.}$ as a function of (hv). The *α value* can be used to compute the $\sigma_{opt.}$ using the next equation [30]:

$$\sigma_{opt.} = \alpha n c \varepsilon_0 = \left. \frac{\alpha n c}{4\pi} \right\} \qquad (14)$$

Where c is the velocity of light. It is shown in Fig. 11 that the films of higher thicknesses have higher optical conductivities in the lower values of wavelength which as we mentioned above may relate to the higher probability of absorption processes.

3.2.4 Energy loss functions

With the dielectric theory system, spectral reaction of this inelastic scattering can be defined as volume energy loss function (VELF) and surface energy loss function (SELF) are given by the following equations [31]:

$$VELF = \frac{\varepsilon_2}{\varepsilon_1^2 + \varepsilon_2^2} \qquad (15)$$

$$SELF = \frac{\varepsilon_2}{(\varepsilon_1 + 1)^2 + \varepsilon_2^2} \qquad (16)$$

The energy dependence of BiI₃ films on the volume and surface energy loss functions is shown in Fig. 12 and Fig.13 respectively.
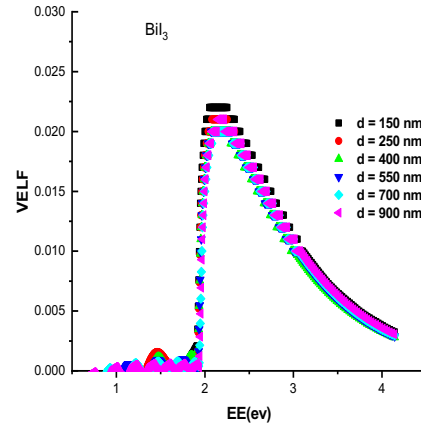

Fig. 12: Dependence of VELF as a function of photon energy, *(hv)* in the fundamental absorption region for investigated thin films.
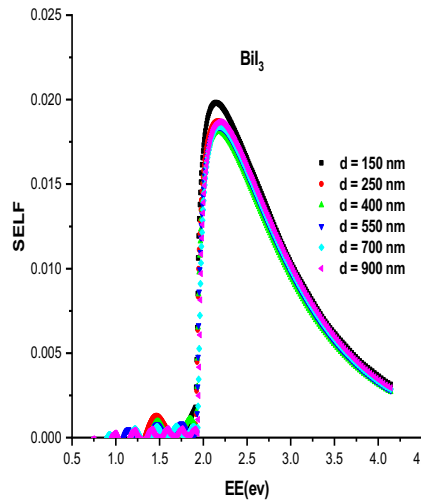

Fig. 13: Dependence of SELF as a function of photon energy, *(hv)* in the fundamental absorption region for investigated thin films.

It can be determined from the figure that the energy loss experienced by the free charge carriers is similar when moving through the volume and the surface. In addition, the maximum value of the loss functions falls roughly to the absorption edge of the BiI₃ films where the inter-band transition is believed to occur. In their observation, Al-Mudhaffer et al. [31] found that the maximum value of VELF and SELF falls around the absorption edge of the film.

3.2.5 Determination of non-linear refractive index

When the film is exposed to strong electric field of incident light, the change in polarizability has to be prolonged by terms proportional to square of electric field. The nonlinear refractive index was deduced in terms of Tichy and Ticha relationship. Tichy and Ticha relationship is a combination of Miller's popularized rule and static refractive index obtained from WDD model as:

$$n_2 = [\frac{12\pi}{n_o}]\chi^{(3)} \tag{17}$$

where $\chi^{(3)}$ is third order non-linear susceptibility. $\chi^{(3)}$ is gotten from the eq. ;

$$\chi^{(3)} = B[\chi^{(1)}]^4 \tag{18}$$

where $\chi^{(1)}$ is linear susceptibility that given by:

$$\chi^{(1)} = \frac{1}{4\pi}[\frac{E_d}{E_o}] \tag{19}$$

Where B= 1.7×10^{-10} (for $\chi^{(3}$ in esu). $\chi^{(3)}$ is given as:

$$\chi^{(3)} = \frac{B}{(4\pi)^4}(n_o^2 - 1)^4 \tag{20}$$

Fig. 14 plots of non-linear refractive index, n_2 versus, λ. From this figure, it is found that value of n_2 reductions with increasing λ for all BiI$_3$ thin films whereas n_2 rises with cumulative the film thickness.
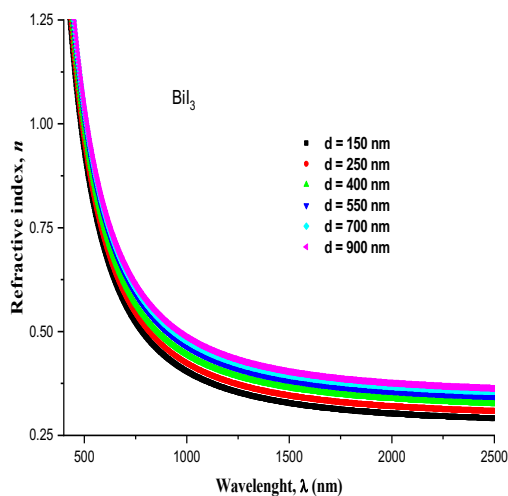

Fig. 14: Dependence of non-linear the refractive index, n_2 on the wavelength for investigated films.

4 Conclusions

BiI$_3$ films with diverse thickness were successfully synthesized using thermal evaporation technique. Structural parameters as crystallite size and microstrain was computed. The findings referred to increasing the crystallite size while the microstrain decrease with increasing film thickness, which is indicated to improving the crystallinity of these films. The effect of film thickness on optical properties BiI$_3$ thin films was investigated. The refractive index and thus extinction coefficient and dielectric constants increased slightly with increasing film thickness. This slight increase was explained in terms of increasing the crystallite size as the film thickness increase. The non-linear refractive index of studied samples was calculated. The n_2 of studied BiI$_3$ films is fit related with the static $n(o)$. in terms of optical parameters in present work, BiI$_3$ films are a valuable as a layer between buffer layer and absorber layer of solar cells and other optoelectronic devices.

References

[1]   M Ruck, J Zeitschrift für Kristallographie, Darstellung und Kristallstruktur von fehlordnungsfreiem Bismuttriiodid, *Crystalline Materials,* **210**. 650-655, (1995).

[2]   Armin Rettenberger, Paul Leiderer, Matthias Probst, Richard Haight, Ultrafast electron transport in layered semiconductors studied with femtosecond-laser photoemission, *Physical Review B,* **56**. 12092, (1997).

[3]   CD England, GE Collins, TJ Schuerlein, NR Armstrong, Epitaxial thin films of large organic molecules: characterization of phthalocyanine and coronene overlayers on the layered semiconductors MoS2 and SnS2, *Langmuir,* **10**. 2748-2756, (1994).

[4]   L Rapoport, Yu Bilik, Yu Feldman, M Homyonfer, SR Cohen, R Tenne, Hollow nanoparticles of WS2 as potential solid-state lubricants, *Nature,* **387**. 791-793, (1997).

[5]   J. J. A. C. Zemann, Crystal structures, *Acta Crystallographica,* **19**. 490-490, (1965).

[6]   H Yorikawa, S Muramatsu, Theoretical study of crystal and electronic structures of BiI3, *Journal of Physics: Condensed Matter,* **20**. 325220, (2008).

[7]   M Schlüter, ML Cohen, SE Kohn, CY Fong, Electronic structure of BiI3, *basic solid state physics,* **78**. 737-747, (1976).

[8]   Yozo Kaifu, Excitons in layered BiI3 single crystals, *Journal of luminescence,* **42**. 61-81, (1988).

[9]   Yōzō Kaifu, Teruo Komatsu, Optical properties of bismuth tri-iodide single crystals. II. Intrinsic absorption edge, *Journal of the Physical Society of Japan,* **40**. 1377-1382, (1976).

[10] Fengxian Ma, Mei Zhou, Yalong Jiao, Guoping Gao, Yuantong Gu, Ante Bilic, Zhongfang Chen, Aijun Du, Single layer bismuth iodide: computational exploration of structural, electrical, mechanical and optical properties, *Scientific reports,* **5**. 1-9, (2015).

[11] L Keller, D Nason, Review of X-ray powder diffraction data of rhombohedral bismuth tri-iodide, *Powder Diffraction,* **11**. 91-96, (1996).

[12] NO Krylova, RI Shekhmametev, M Yu Gurgenbekov, Indirect transitions and the optical spectrum of BiI 3 crystals at low temperatures, *Optics and Spectroscopy,* **38**. 545-547, (1975).

[13] H Kondo, T Kawai, T Karasawa, I Akai, T Komatsu, Lateral transport and dynamical behavior of quasi-two-dimensional excitons at high density along a stacking disorder plane in layered BiI3 crystals, *Journal of luminescence,* **66**. 448-452, (1995).

[14] Nikolas J Podraza, Wei Qiu, Beverly B Hinojosa, Haixuan Xu, Michael A Motyka, Simon R Phillpot, James E Baciak, Susan Trolier-McKinstry, Juan C Nino, Band gap and structure of single crystal BiI3: Resolving discrepancies in literature, *Journal of Applied Physics,* **114**. 033110, (2013).

[15] Azaree T Lintereur, Wei Qiu, Juan C Nino, James Baciak, Characterization of bismuth tri-iodide single crystals for wide band-gap semiconductor radiation detectors, *Nuclear Instruments and Methods in Physics Research Section A: Accelerators, Spectrometers, Detectors and Associated Equipment,* **652**. 166-169, (2011).

[16] Paul J Sellin, Thick film compound semiconductors for X-ray imaging applications, *Nuclear Instruments and Methods in Physics Research Section A: Accelerators, Spectrometers, Detectors and Associated Equipment,* **563**. 1-8, (2006).

[17] Alka Garg, Monika Tomar, Vinay Gupta, Synthesis and characterisation of thin films of bismuth triiodide for semiconductor radiation detectors, *in Conference Papers in Science.* Hindawi.2014.

[18] Muvva D Prasad, LD Varma Sangani, Sudip K Batabyal, M Ghanashyam Krishna, Single and twinned plates of 2D layered BiI 3 for use as nanoscale pressure sensors, *CrystEngComm,* **20**. 4857-4866, (2018).

[19] Qi Wei, Jinhui Chen, Ping Ding, Bo Shen, Jiang Yin, Fei Xu, Yidong Xia, Zhiguo Liu, Synthesis of easily transferred 2D layered BiI3 nanoplates for flexible visible-light photodetectors, *ACS applied materials & interfaces,* **10**. 21527-21533, (2018).

[20] ER Shaaban, Optical constants and fitted transmittance spectra of varies thickness of polycrystalline ZnSe thin films in terms of spectroscopic ellipsometry, *Journal of alloys and compounds,* **563**. 274-279, (2013).

[21] D Nason, Ludwig Keller, The growth and crystallography of bismuth tri-iodide crystals grown by vapor transport, *Journal of crystal growth,* **156**. 221-226, (1995).

[22] Essam R Shaaban, Ishu Kansal, SH Mohamed, Joés MF Ferreira, Microstructural parameters and optical constants of ZnTe thin films with various thicknesses, *Physica B: Condensed Matter,* **404**. 3571-3576, (2009).

[23] Sapan Kumar Sen, Utpal Chandra Barman, MS Manir, Pritish Mondal, Supria Dutta, Mollika Paul, MAM Chowdhury, MA Hakim, X-ray peak profile analysis of pure and Dy-doped α-MoO3 nanobelts using Debye-Scherrer, Williamson-Hall and Halder-Wagner methods, *Advances in Natural Sciences: Nanoscience and Nanotechnology,* **11**. 025004, (2020).

[24] Jing-quan Zhang, Liang-huan Feng, Wei Cai, Jia-gui Zheng, Ya-ping Cai, Bing Li, Li-li Wu, Ye Shao, The structural phase transition and mechanism of abnormal temperature dependence of conductivity in ZnTe: Cu polycrystalline thin films, *Thin Solid Films,* **414**. 113-118, (2002).

[25] R Swanepoel, Determination of the thickness and optical constants of amorphous silicon, *Journal of Physics E: Scientific Instruments,* **16**. 1214, (1983).

[26] E Marquez, JB Ramirez-Malo, P Villares, R Jimenez-Garay, R Swanepoel, Optical characterization of wedge-shaped thin films of amorphous arsenic trisulphide based only on their shrunk transmission spectra, *Thin Solid Films,* **254**. 83-91, (1995).

[27] Cristian Baban, GI Rusu, On the structural and optical characteristics of CdSe thin films, *Applied surface science,* **211**. 6-12, (2003).

[28] M Nowak, Linear distribution of intensity of radiation reflected from and transmitted through a thin film on a thick substrate, *Thin Solid Films,* **266**. 258-262, (1995).

[29] TS Moss:, Optical Properties of Semi-conductors, , *Butterworths scientific Publications, London,* **14**. 496-497, (1959).

[30] Jacques I Pankove, Optical processes in semiconductors, *Courier Corporation*1975.

[31] Mohammed F Al-Mudhaffer, Maged A Nattiq, Mohammed Ali Jaber, Linear optical properties and energy loss function of Novolac: epoxy blend film, *Archives of Applied Science Research* **4**. 1731-7140, (2012).